RSC Advances

PAPER

View Article Online
View Journal | View Issue

Cite this: *RSC Adv.*, 2022, **12**, 475

A novel colorimetric and fluorescent probe based on a core-extended perylene tetra-(alkoxycarbonyl) derivative for the selective sensing of fluoride ions†

Yongshan Ma,* Yanzhao Xia, Yanyan Zhu, Fengxia Zhang,* Jingcheng Cui, Tianyi Jiang, Xiangfeng Jia and Xuemei Li

Received 14th October 2021
Accepted 4th December 2021

DOI: 10.1039/d1ra07596a

rsc.li/rsc-advances

A novel fluoride (F^-) colorimetric and fluorescent probe (**P1**) based on a core-extended perylene tetra-(alkoxycarbonyl) (PTAC) derivative was developed. The probe exhibited high sensitivity and selectivity for distinguishing F^- from other common anions through significant changes of the UV-Vis and fluorescence spectra. Job's plot analysis revealed that the stoichiometry of the **P1**–F^- interaction is 1 : 1. The association constant between **P1** and F^- was estimated to be 9.7×10^2 M^{-1} and the detection limit of F^- was about 0.97 μM. An approximately 76 nm red-shift in the absorption and fluorescent quenching response was observed when F^- was associated with **P1**. The emission intensity (I_{574}) decreased linearly along with the F^- concentration from 3×10^{-5} M to 2×10^{-4} M. The mechanism of intermolecular proton transfer (IPT) was deduced based on the changes in the absorption, fluorescence, electrochemistry, and ^{1}H NMR titration spectra. The density functional theory (DFT) theoretical results of the **P1**–F^- complex are in good agreement with the experimental results. The rapid detection of F^- ions in the solid state and living cells was also studied.

1. Introduction

The construction of organic molecular scaffolds with high selectivity and sensitivity for anion recognition is a research hotspot in supramolecular chemistry.[1,2] Among the various types of anions, fluoride (F^-) ions receive lots of attention because they play important roles in several environmental, biological and industrial processes.[3–5] For example, F^- is important for preventing enamel demineralization and dental caries caused by the use of orthodontic appliances, and is also used to treat osteoporosis.[6,7] However, high intake of F^- from drinking water is known to cause fluorosis, urolithiasis, nephrotoxic changes, and even cancer.[8–10] The United States Environmental Protection Agency (EPA, USA) has recommended an allowable F^- concentration of 2 ppm in water.[11] Therefore, it is important to develop tools for the effective detection of F^- anions. The quantitative analysis of F^- can be performed by ion chromatography, ion-selective electrodes, and standard Willard–Winter methods. However, these methods have limitations like low mobility, high cost or complicated procedures.[12] Thus, highly sensitive, selective, rapid, and convenient F^- detection methods need be further developed. Efforts have been devoted to discovering effective fluorescent probes for F^- because they have outstanding sensitivity, short response time, and are non-damaging and non-invasive.[13,14]

Perylene diimides (PDIs) have been widely used as industrial pigments.[15] Their application as fluorescent probes has received great attention in recent years because of their exceptional photo, thermal, chemical, and weather stability.[16–18] However, due to the aggregation of the perylene core, many PDIs have poor solubility and weak fluorescence, which limit their applications.[19] Perylene tetra-(alkoxycarbonyl) (PTAC) has four electron-deficient carboxylic ester chains attached to the perylene core, and shows excellent solubility and fluorescence in organic solvents.[20] In order to further improve the optical and electronic properties of PTAC, the development of core-extended PTAC derivatives has been conducted in the past decade.[21,22] PTAC fluorescent probes containing heteroatoms, such as S- and O-, and N-heterocycles in the perylene skeleton have been explored.[23–25]

In the past few decades, the feasibility of using N–H units, including amide, amine, pyrrole, imidazole, indole, and urea/thiourea, in probes to bind F^- through hydrogen bonding interactions has been well demonstrated.[26–28] Recently, we reported PTAC-based F^- probes in which the hydrogen bond donor chloroacetamide fragment was directly attached to the perylene core. An intermolecular proton-transfer (IPT) process

School of Municipal and Environmental Engineering, Shandong Jianzhu University, Jinan 250101, Shandong, China. E-mail: mlosh@sdjzu.edu.cn; zhangfengxia19@sdjzu.edu.cn

† Electronic supplementary information (ESI) available. See DOI: 10.1039/d1ra07596a

between F^- and H atom at the amide N position played a key role in their sensing properties.[29] Herein, we describe a novel core-extended PTAC derivative (**P1**) (Scheme 1) that can be used as a colorimetric and fluorescent probe for F^- detection. **P1** showed an obvious color change and drastic fluorescence quenching in the presence of F^- ions. These optical properties arose from the IPT process between F^- and the H atom of an N–H group, which resulted in efficient intramolecular charge-transfer (ICT) transition from the N˙ moiety to perylene, and caused an observed red-shifted absorption spectrum for the probe. This is the first example of a PTAC probe containing a seven-atoms ring in the perylene bay position. This study is expected to provide guidance for the design of a novel perylene fluorescent F^- probe.

2. Experimental methods

2.1. Materials and instrumental methods

All the chemical reagents were analytically pure, obtained from commercial sources, and used directly without further purification. Tetrabutylammonium salts (purchased from Aladdin, Shanghai, China) were used for the anion studies. ^{1}H NMR and ^{13}C NMR spectra were obtained on a Bruker Advance 400 spectrometer in $CDCl_3$ at room temperature. FT-IR spectra were obtained using a Bruker Tensor-27 spectrophotometer. Mass spectra were recorded on a Bruker Maxis UHR-TOF MS spectrometer. Electrochemistry was measured using a CH 1604C electrochemical analyzer, employing glassy carbon (diameter: 1.6 mm; area 0.02 cm^2), a platinum wire, and $Ag/AgNO_3$ (Ag/Ag^+) as the working electrode, counter electrode, and reference electrode, respectively. Tetrabutylammonium hexafluorophosphate ($TBAPF_6$) (0.1 M) in dichloromethane was used as the electrolyte. UV-vis absorption spectra were obtained with an Agilent Cary 5000 spectrophotometer. Fluorescence spectra measurements were obtained on a Hitachi F-7100 spectrofluorometer. The solutions of the probes were typically 1×10^{-5} M for the UV-vis and emission studies. Fluorescence microscopic images were obtained using an Olympus (Japan) BH2 fluorescence microscope with an excitation range of 450–490 nm.

2.2. Molecular details

Both the structure optimization and property calculations were determined through the Becke's three-parameter gradient-corrected hybrid density function B3LYP method and the standard 6-31G* basis set. All the calculations were performed using the Gaussian 03 program installed on a Windows PC.[30–32]

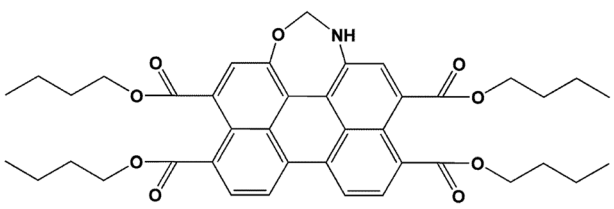

Scheme 1 Structure of **P1**.

2.3. Live cell imaging

Human lung cancer A549 cells, obtained from the Chinese Type Culture Collection (Shanghai Institute of Cell Biology, Chinese Academy of Science, China), were cultured in Dulbecco's modified Eagle's medium (DMEM) containing 10% fetal bovine serum (FBS) and streptomycin/penicillin (100 U mL^{-1}) in a humidified incubator at 37 °C and 5% CO_2. After confluence, the cells were separated with trypsin solution, rinsed with DMEM, centrifuged at 125 g for 3 min, and then resuspended and subcultured according to the standard protocol. The culture medium was removed, and A549 cells were incubated with **P1** (50 μM in DMSO buffered with PBS, pH = 7.54) at 37 °C for 20 min. After washing with PBS three times to remove excess **P1**, the cells were further incubated with F^- (1.5 mM in H_2O) at 37 °C for 10 min and imaged using an Olympus BH2 fluorescence microscope.

2.4. Synthesis and characterization

Scheme S1† outlines the synthesis of the seven-numbered heterocycle annulated PTAC derivative **P1**. It was prepared according to a published procedure.[33] Compound **3** (1.0 g, 1.44 mmol), zinc powder (0.5 g, 8.0 mmol), and ammonium chloride (0.8 mg, 16.0 mmol) were dissolved in 100 mL tetrahydrofuran (THF). After the mixture was stirred at room temperature for 3 h, the ammonium chloride and zinc powder were collected by filtration. The crude product was purified by silica gel column chromatography to give a dark brown solid as the compound **2** (0.76 g, 80%). Compound **2** (0.4 g, 5.0 mmol), paraformaldehyde (0.12 g, 4.0 mmol), and catalyzed formic acid were dissolved in 100 mL ethanol under air. The solution was refluxed for 12 h. The precipitate was collected by filtration. The crude product was purified by silica gel column chromatography (eluent: 2% ethyl acetate in dichloromethane) to give a red solid as the pure **P1** (0.25 g, 62%, mp: 300–302 °C). ^{1}H NMR (400 MHz, $CDCl_3$, δ ppm): 8.17 (d, 1H, J = 7.7 Hz), 7.98 (d, 1H, J = 7.7 Hz), 7.91 (d, 1H, J = 7.2 Hz), 7.88 (s, 1H), 7.80 (s, 1H), 7.52 (s, 1H), 6.00 (m, 1H), 5.03 (d, 2H, J = 7.2 Hz), 4.34 (m, 8H), 1.80–1.73 (m, 8H), 1.57–1.46 (m, 8H), 1.02–0.98 (m, 12H) (Fig. S1†). ^{13}C NMR (100 MHz, $CDCl_3$, δ ppm): 169.01, 168.96, 168.03, 167.82, 157.15, 144.18, 131.76, 129.47, 128.45, 125.67, 122.15, 120.82, 79.45, 65.37, 65.29, 65.25, 65.21, 30.70, 30.68, 30.62, 29.72, 19.31, 19.26, 13.85 (Fig. S2†). FT-IR (KBr, cm^{-1}): 3380, 2958, 2863, 1707, 1611, 1525, 1449, 1382, 1240, 1191, 1154, 1058, 953, 904, 828, 800, 742, 494, 427 (Fig. S3†). HRMS: $C_{41}H_{45}NO_9$ (M^-), calcd, 695.3094; found 694.2994 (Fig. S4†).

3. Results and discussion

3.1. Absorption spectral response toward F^-

The carboxylic ester chain connected to the perylene core increased the solubility of perylene derivatives in organic solutions, but a satisfactory water solubility was still lacking. The interaction between **P1** and anions was studied by spectrophotometric titration by adding the standard solution of tetrabutylammonium salt into a CH_2Cl_2 solution of **P1**. The free **P1** had an intense absorption band at 501 nm and a weak absorption

band at 379 nm (Fig. 1a). The main band at 501 nm ($\varepsilon = 13\ 100$ L mol^{-1} cm^{-1}) was a typical π–π^* transition absorption band for PDI dyes.[34] When F^- (0–30.0 equiv.) was added into the solution of **P1**, the intensity bands at 501 and 379 nm decreased gradually, and new bands appeared at 577 and 413 nm, which were caused by the hydrogen binding interaction between N–H of **P1** and F^- anions. The light orange-yellow color of the probe solution turned to blue-gray (Fig. 1a inset). Two well-defined isosbestic points were observed at 436 and 530 nm, indicating that a new species was formed when **P1** was treated with F^-. From the Job's plot, it could be determined that the stoichiometry of the **P1**–F^- interaction was 1 : 1 (Fig. S5†).

Analogous investigations were carried out with a variety of anions, such as Cl^-, Br^-, I^-, SO_4^{2-}, AcO^-, ClO_4^-, and $H_2PO_4^-$. After adding 100 equiv. of these anions, the absorption spectra of **P1** showed no obvious change (Fig. 1b inset). It was noteworthy that the absorption band was not altered by the anions with weak alkalinity, such as Cl^-, Br^-, I^-, SO_4^{2-}, AcO^-, ClO_4^-, and $H_2PO_4^-$. These results provide strong evidence that the red-shifted peak at 577 nm was caused by the N–H deprotonation of **P1**. The association constant (K_a) between **P1** and F^- was estimated to be 9.7×10^2 M^{-1} by the Benesi–Hildebrand method (Fig. S6†).[35] Moreover, the limit of detection (LOD) of F^- was about 0. 97 μM (*i.e.* 0.018 ppm), which was well below 2 ppm (the allowed concentration level in drinking water set by the USEPA).[36] All the above measurements were completed within 10 s, indicating that the probe had a real-time capability.

3.2. Fluorescence response toward F^-

The F^- ions binding properties of **P1** were then studied in CH_2Cl_2 solution by emission spectroscopy. Upon excitation at 501 nm, the free **P1** showed a maximum fluorescence emission peak at 574 nm due to an efficient photoinduced-electron-transfer (PET) process from the lone pair of electrons (seven-atom ring moiety) to the excited perylene fluorophore. With the increase in F^- concentration, the fluorescence of **P1** at 574 nm decreased gradually (Fig. 2a). Fig. 2b shows the correlation between the emission response of **P1** at 574 nm and F^- concentration in CH_2Cl_2. The emission intensity (I_{574}) decreased linearly along with the increase in F^- concentration from 3×10^{-5} M to 2×10^{-4} M (Fig. S7†). The linear fitting equation was $y = -77.8x + 1937.8$, where y is the fluorescence intensity of 574 nm and x is the concentration of F^-. The F^--sensing process could be clearly seen not only by the color change under ambient light but also by the bright fluorescence under a UV lamp. During the fluorometric titration of **P1** with F^- ions, the bright orange-yellow color solution of **P1** turned to deep blue (Fig. 2a inset). These results met our expectation that **P1** could be used as a sensitive naked-eye probe for F^- ions.

To study the photostability of **P1** in CH_2Cl_2 solution, we monitored the fluorescence spectra of **P1** under continuous 300 W Xe lamp irradiation. After irradiation for 20 min, the fluorescence intensity remained unchanged, which proved that **P1** had high photostability. To evaluate the selectivity of **P1** for the detection of F^-, competitive experiments were also carried out with 30 equiv. of F^- and 100 equiv. of various other anions (Cl^-, Br^-, I^-, SO_4^{2-}, AcO^-, ClO_4^-, and $H_2PO_4^-$). The fluorescence spectra of **P1** and F^- were not significantly affected by the subsequent addition of competing anions, and the fluorescence switching behavior was not affected even when all the anions existed simultaneously (Fig. 3). The experimental results showed that **P1** could have high selectivity for F^- in colorimetric and fluorescent sensors.

3.3. Electrochemical response toward F^-

The F^- binding site (N–H moiety) was directly attached to the redox active perylene moiety, and any small perturbation in the electron density of the N–H moiety (by forming H-bond with F^-) may result in a significant change in the redox property of the perylene moiety. Therefore, the electrochemical properties of **P1** in CH_2Cl_2 solution, in the absence and presence of F^- ions, were studied by differential pulse voltammetry (DPV) technique (Fig. 4). It was clear from the figure that **P1** exhibited two reduction peaks characterized by the perylene moiety. The first peak (−0.902 V) corresponded to the formation of radical anions, and the second peak (−1.242 V) belonged to the

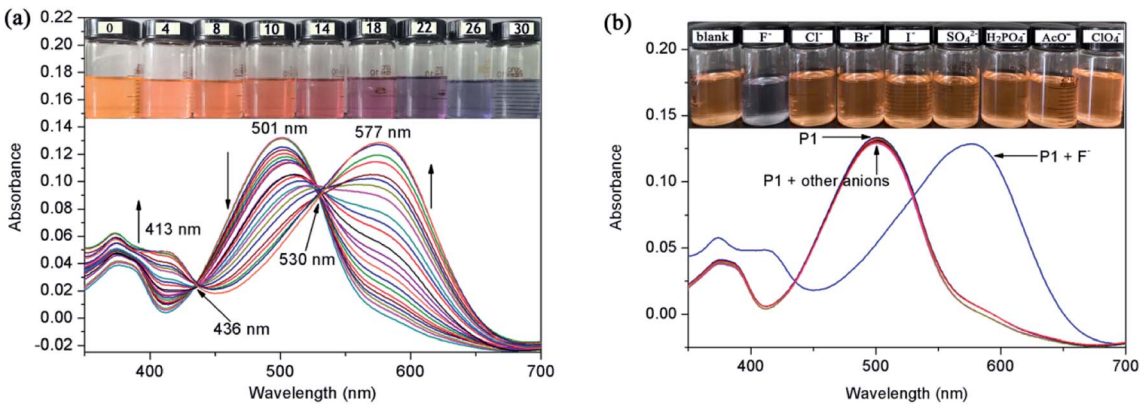

Fig. 1 (a) Absorption spectra changes of **P1** (10 μM) in CH_2Cl_2 solution in the presence of F^- ions only (0–30 equiv.). (b) Absorption spectra of **P1** (10 μM) in CH_2Cl_2 solution in the presence of various anions (100 equiv.). The inset shows a photograph of visible color under ambient light.

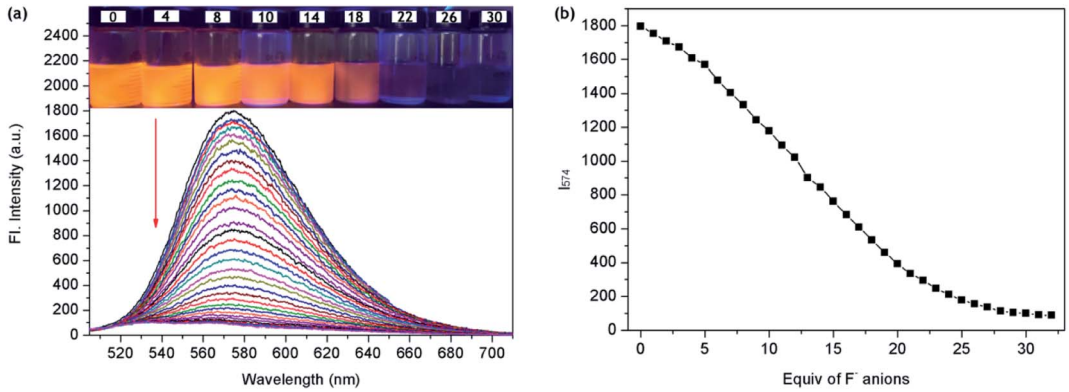

Fig. 2 (a) Fluorescence changes of **P1** (10 μM, excitation at 501 nm) in CH_2Cl_2 solution in the presence of 0–30 equiv. of F^-. The inset shows a photograph of visual fluorescence color under a hand-held UV lamp. (b) The fluorescence intensity ($I_{574\ nm}$) as a function of equiv. of F^- anions.

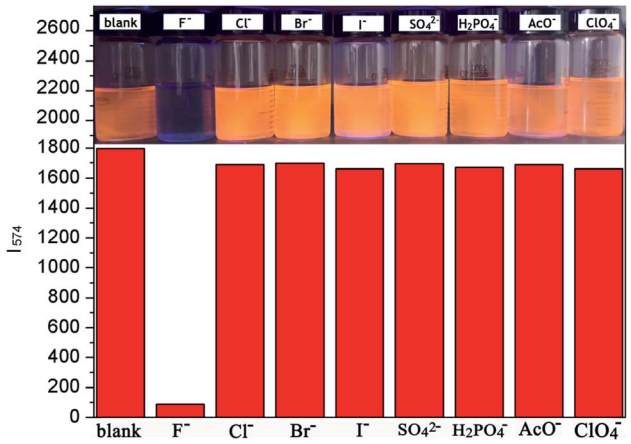

Fig. 3 Fluorescence changes of **P1** (10 μM) after treatment with various relevant analytes (30 equiv. for F^-, 100 equiv. for other anions) in CH_2Cl_2 solution. The inset shows a photograph of the visual fluorescence color under a hand-held UV lamp.

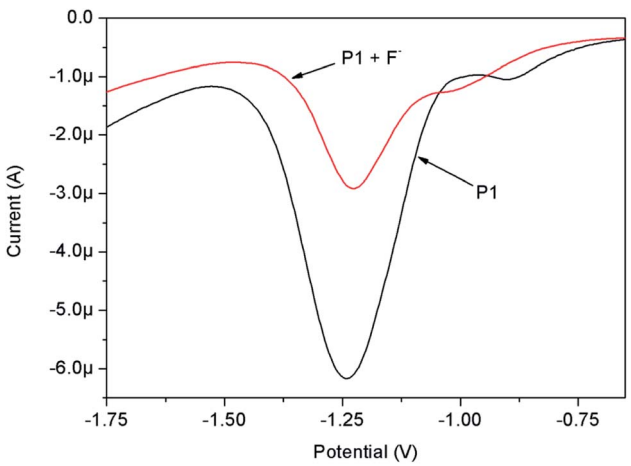

Fig. 4 Redox property changes of **P1** in CH_2Cl_2 upon addition of F^- ions.

formation of dianions.[37] The first reduction potential of **P1** was shifted toward a more negative value (−1.017 V) by introducing strong electron-withdrawing F^- ions. The addition of F^- made the electron reduction in perylene more difficult than in the free probe. This was due to the fact that the complexation of the N–H group with F^- ions, through H-bonding, made the (–N^-–CH_2–O–) group relatively electron rich and thus increased the intensity of ICT transition from the (–N^-–CH_2–O–) moiety to the perylene core, and consequently made it difficult to reduce **P1**. The peak current decreased with the addition of F^- ions, suggesting that the formed **P1**–F^- complex had a lower diffusion coefficient. Elango reported a similar electrochemical behavior of probes containing N–H groups in the presence of F^-.[38]

3.4. Visual detection of F^- in the solid state

In order to explore the potential application of **P1** in the solid state, fluorescence microscopy was used to test the utility of **P1** in F^--dependent fluorescence imaging. As shown in Fig. 5, a quantifiable 10 mM solution of **P1** was adsorbed on a glass coverslip, and revealed bright red fluorescence under excitation with a blue-filter source of 460–490 nm. Upon the addition of an F^- ions spot (30 mM), it was adsorbed on the glass coverslip, changing the color of the center to a weak red fluorescence. To check the feasibility of using silica-coated plates, these plates were dropped in a quantifiable **P1** solution (10 mM) and then dried in air. When different concentrations of F^- solution were dropped on the plates, a distinct color change from light yellowish-orange to undertint was immediately observed under UV light ($\lambda_{ex} = 365$ nm) (Fig. 6). Competitive anions did not have a significant influence on F^- detection in the silica-coated plates. Therefore, **P1** was a prospective probe for detecting F^- ions in the solid state. These studies strengthen the possibility of **P1** being used as a candidate probe for the rapid and convenient detection of F^- ions.

3.5. Nature of the interaction between P1 and F^-

In order to further understand the actual mechanism of the interaction between **P1** and F^-, ^{1}H NMR studies were carried out in $CDCl_3$ (Fig. 7). It was found that free **P1** showed

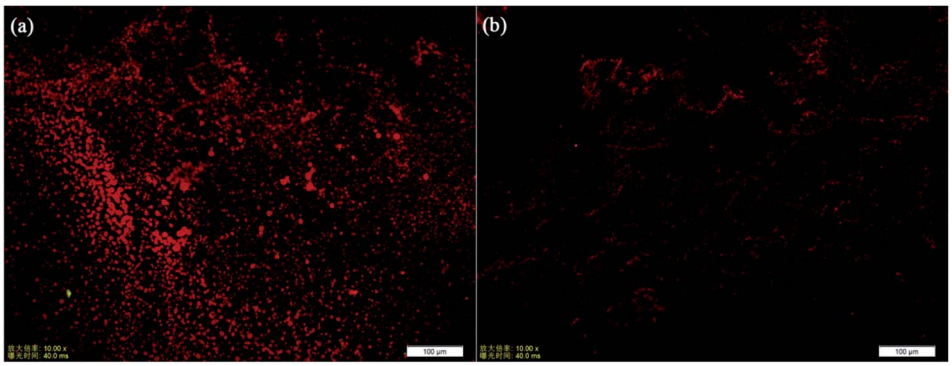

Fig. 5 Fluorescence microscopic images of **P1** (a) before and (b) after the addition of F^- ions deposited on a glass slide.

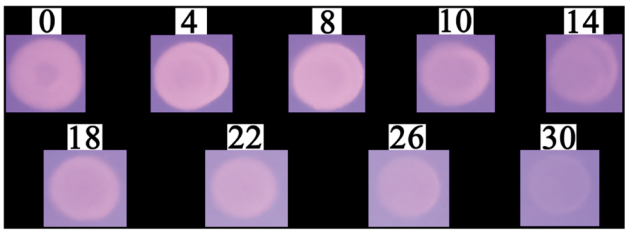

Fig. 6 Fluorescence response of **P1** to F^- ions (0–30 equiv.) on silica-coated slides under a hand-held UV lamp.

resonance for the N–H proton at δ = 5.98 ppm. Upon the addition of F^- to **P1**, the peak corresponding to the N–H proton moved downfield and broadened, and finally disappeared. After the addition of 30 equiv. of F^-, a new triplet signal appeared at 15.85 ppm, indicating the formation of an HF_2^- dimer.[39] The presence of this new species indicated the deprotonation of the NH group. These results indicated that the binding between **P1** and F^- was formed through H-bonding between H^+ (N–H proton) and F^- (N–H···F^-). The formation of the H-bond followed by deprotonation of the N–H fragment would increase the electron density of the seven-atoms ring moiety, which facilitated the ICT transition from the seven-atoms ring moiety to the perylene moiety, and consequently caused the red-shift of λ_{ICT} and the obvious color change.

3.6. Quantum chemistry computation

To gain further insight into the sensing mechanism, geometry optimization and quantum chemical calculations for **P1** and **P1**–F^- complex were investigated using density functional theory (DFT) implanted in the Gaussian 03 program employing the basis set B3LYP/6-31G. As shown in Fig. 8, the probe **P1**

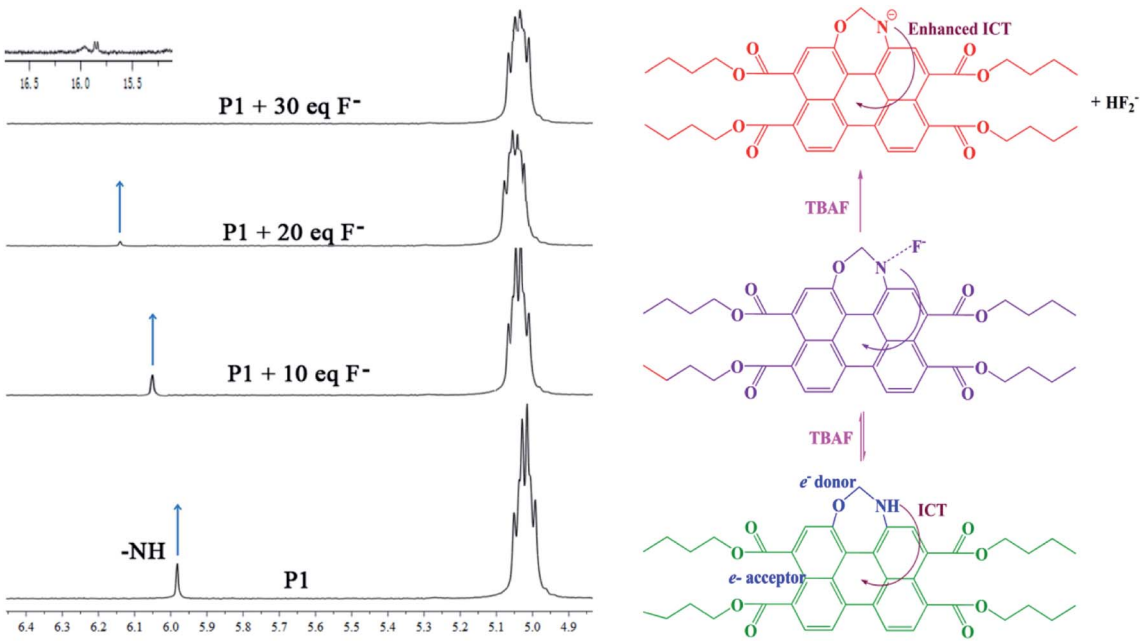

Fig. 7 Partial ^{1}HNMR spectra of **P1** in the presence of TBAF in $CDCl_3$.

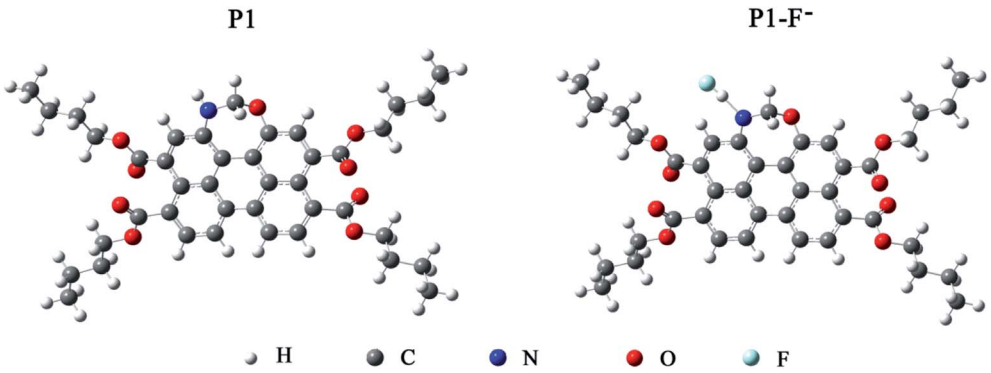

Fig. 8 Optimized structures of **P1** and **P1**–F^-.

bonded F^- at the N–H position of the seven-atoms ring group. After being captured by F^-, the N–H bond of **P1** was obviously elongated from 1.012 to 1.536 Å, and the distance between active proton and F^- was 1.005 Å. Moreover, the angle of the N–N–C in the seven-atoms ring moiety decreased from 122.7° to 120.6°. These results indicated that the strong H–F interaction may lead to the deprotonation of **P1**, and the lone pair electrons in the nitrogen atom may increase the electron density of the seven-atoms ring moiety and facilitate ICT transition. The deprotonation also caused a new absorption band with a red-shift of 76 nm.

The electron density distributions of the HOMO and LUMO of **P1** and its F^- ions complex are shown in Fig. 9. As expected, the electron density in the HOMO was mainly distributed on the seven-atoms ring moiety, while the LUMO was located on the perylene moiety in the free probe, which clearly indicated that **P1** was an ICT probe.[40] The HOMO/LUMO energy levels of **P1** and **P1**–F^- were estimated to be −5.12/−2.31 eV and −1.71/−0.52 eV, respectively. The energy gap ΔE ($= E_{HOMO} - E_{LUMO}$) determined the ease of ICT from the HOMO to the LUMO. In all the cases, the observed red-shifts in the electronic spectra indicated that the binding of F^- ion caused a conformational change affecting the HOMO level. Electrochemical experiments showed that the LUMO energy increased with the cathodic-shift of the reduction potential.[41] The binding of F^- ion to **P1** had effects on both the HOMO and LUMO energy, and the ΔE of the **P1**–F^- complex was relatively low. Thus, the theoretical results were in good agreement with the experimental results for the **P1**–F^- complex.

3.7. Application in live cell imaging

The cell permeability and F^--sensing ability of **P1** in the human lung cancer A549 cell line were further determined. Strong intracellular fluorescence was observed when A549 cells were incubated with **P1** (50 μM in DMSO, pH = 7.4) at 37 °C for

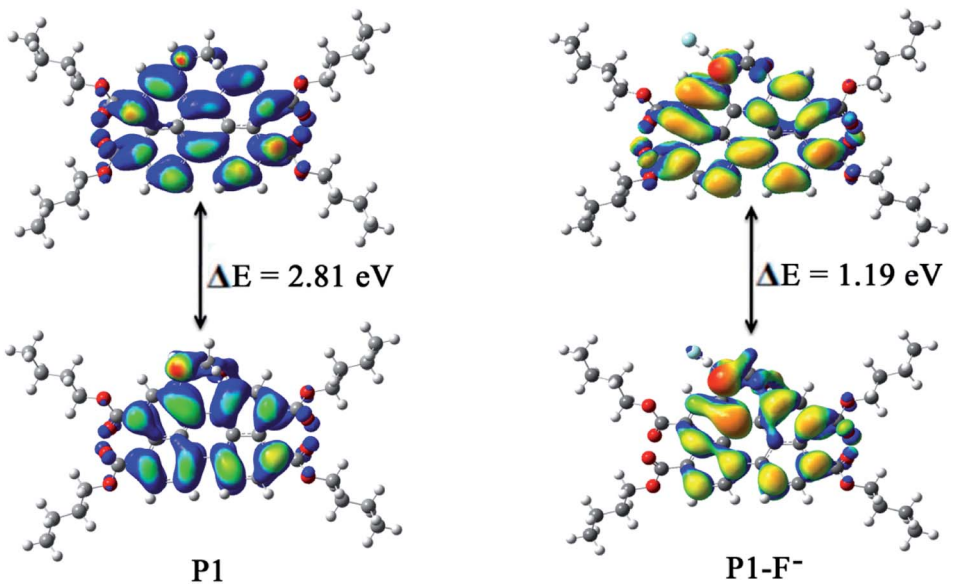

Fig. 9 Energy diagrams of HOMO (down) and LUMO (up) orbitals of **P1** and the formation of the **P1**–F^- complex.

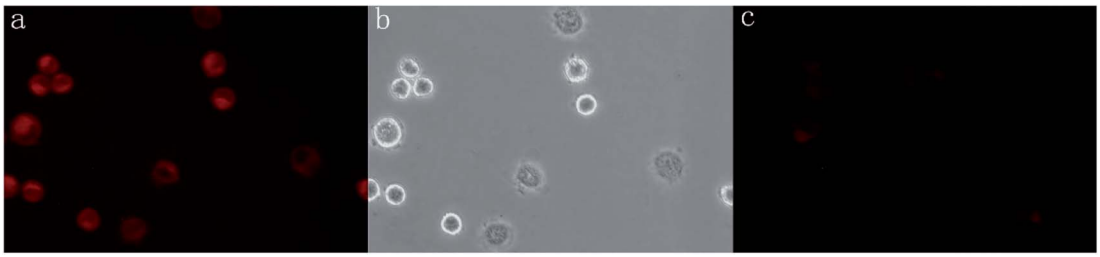

Fig. 10 (a) Fluorescence images of A549 cells stained with **P1** (50 μM) for 20 min at 37 °C, (b) merged bright field images of A549 cells and (c) fluorescence image of A549 cells incubated with **P1** (50 μM) and subsequently treated with NaF (1.5 mM) for 10 min.

20 min (Fig. 10a). After being treated with the probe, the cells remained intact morphologically (Fig. 10b). When the same cells were further incubated with 1.5 mM NaF in PBS buffer at 37 °C for 10 min, no significant fluorescence was observed inside the cells (Fig. 10c). These results indicated the abilities of **P1** to permeate living cell membranes and sense intracellular F^- ions.

4. Conclusions

In this study, a colorimetric and fluorescent F^- probe was developed based on a core-extended PTAC derivative. The IPT process between F^- and H atom (at the N position of the seven-atom ring moiety) and the subsequent ICT transition from the N˙ moiety to the perylene moiety played a key role in its sensing performance. The F^--ions sensing *via* H-bonding interaction could be easily monitored by absorption, fluorescence and ^1H NMR spectral techniques as well as by electrochemical studies. The probe could also be utilized for the fluorescence imaging of F^- in the solid state and in live cells. This is the first example of a PTAC probe containing a seven-atoms ring in the perylene bay position. This novel design strategy would be helpful for the development of chemical probes for F^- ions.

Conflicts of interest

There are no conflicts to declare.

Acknowledgements

This work was supported by the Shandong Provincial Natural Science Foundation (ZR2020MB086, ZR2020MD115), the Doctoral Research Fund of Shandong Jianzhu University (XNBS1712, XNBS1938), the Youth Innovation Technology Project of Higher School in Shandong Province (2019KJD003), and National Natural Science Foundation of China (81903370).

References

1 N. Borah, B. Nayak, A. Gogoi and G. Das, A benzimidazole-based non-symmetrical tripodal receptor for the ratiometric fluorescence sensing of fluoride ions and solid state recognition of sulfate ions, *New J. Chem.*, 2019, **43**, 16497–16505.

2 A. K. Mahapatra, R. Maji, K. Maiti, S. S. Adhikari, C. D. Mukhopadhyay and D. Mandal, Ratiometric sensing of fluoride and acetate anions based on a BODIPY-azaindole plateform and its application to living cell imaging, *Analyst*, 2014, **139**, 309–317.

3 X. Xu, Y. Chen, L. Wei, W. Mao, F. Lin and X. Zhou, Fluorescent turn-on probes for the detection of fluoride ions in organic solvent and in cells, *Anal. Methods*, 2016, **8**, 245–248.

4 B. Ke, W. Chen, N. Ni, Y. Cheng, C. Dai, H. Dinh and B. Wang, A fluorescent probe for rapid aqueous fluoride detection and cell imaging, *Chem. Commun.*, 2013, **49**, 2494–2496.

5 B. Aradhyula, R. Chinta, K. jayarao and K. Venkatasubbaiah, Synthesis and characterization of poly(tetraphenylimidazole) s and their application in the detection of fluoride ions, *RSC Adv.*, 2020, **10**, 13149–13154.

6 X. Yang, L. Zheng, L. Xie, Z. Liu, Y. Li, R. Ning, G. Zhang, X. Gong, B. Gao, C. Liu, Y. Cui, G. Sun and G. Zhang, Colorimetric and on-off fluorescent chemosensor for fluoride ion based on diketopyrrolopyrrole, *Sens. Actuators, B*, 2015, **207**, 9–24.

7 A. Roy, D. Kand, T. Saha and P. Talukdar, Pink fluorescence emitting fluoride ion sensor: investigation of the cascade sensing mechanism and bioimaging applications, *RSC Adv.*, 2014, **4**, 33890–33896.

8 K. Dhanunjayarao, V. Mukundam and K. Venkatasubbaiah, A highly selective ratiometric detection of F^- based on excited-state intramolecular proton-transfer (imidazole) materials, *J. Mater. Chem. C*, 2014, **2**, 8599–8606.

9 Y. Zheng, Y. Duan, K. Ji, R. Wang and B. Wang, Tuning the reaction rates of fluoride probes for detection in aqueous solution, *RSC Adv.*, 2016, **6**, 25242–25245.

10 A. Roy, A. Datar, D. Kand, T. Saha and P. Talukdar, A fluorescent off–on NBD-probe for F^- sensing theoretical validation and experimental studies, *Org. Biomol. Chem.*, 2014, **12**, 2143–2149.

11 R. Gupta, R. Ali, S. Razi, P. Srivastava, S. Dwivedi and A. Misra, Synthesis and application of a new class of D–π–A type charge transfer probe containing imidazole – naphthalene units for detection of F– and CO_2, *RSC Adv.*, 2017, **7**, 4941–4949.

12 M. Yuan, Q. Wang, W. Wang, D. Wang, J. Wang and J. Wang, Truxene-cored π-expanded triarylborane dyes as single- and

two-photon fluorescent probes for fluoride, *Analyst*, 2014, **139**, 1541–1549.

13 S. Park, N. Kwon, J. Lee, J. Yoon and I. Shin, Synthetic ratiometric fluorescent probes for detection of ions, *Chem. Soc. Rev.*, 2020, **49**, 143–179.

14 T. Jayeoye and T. Rujiralai, Sensitive and selective colorimetric probe for fluoride detection based on the interaction between 3-aminophenylboronic acid and dithiobis(succinimidylpropionate) modified gold nanoparticles, *New J. Chem.*, 2020, **44**, 5711–5719.

15 C. Li and H. Wonneberger, Perylene imides for organic photovoltaics: yesterday, today, and tomorrow, *Adv. Mater.*, 2012, **24**, 613–636.

16 Z. J. Chen, L. M. Wang, G. Zou, L. Zhang, G. J. Zhang, X. F. Cai and M. S. Teng, Colorimetric and ratiometric fluorescent chemosensor for fluoride ion basedon perylene diimide derivatives, *Dyes Pigm.*, 2012, **94**, 410–415.

17 K. M. Dibakar, R. Subhasish, D. Ayan and B. Arindam, Aqueous fluoride ion sensing by a new perylenediimide derivative: Interaction between the hydrated fluoride and the aromatic molecule, *Chem. Phys. Lett.*, 2013, **588**, 76–81.

18 Y. F. Wang, L. Zhang, G. J. Zhang, Y. Wu, S. Y. Wu, J. J. Yu and L. M. Wang, A new colorimetric and fluorescent bifunctional probe for Cu^{2+} and F^{-} ions based on perylene bisimide derivatives, *Tetrahedron Lett.*, 2014, **55**, 3218–3222.

19 S. Chen, P. Slattum, C. Wang and L. Zang, Self-assembly of perylene imide molecules into 1D nanostructures: methods, morphologies, and applications, *Chem. Rev.*, 2015, **115**, 11967–11998.

20 M. Takahashi, K. Asaba, T. Lua, T. Inuzuka, N. Uemura, M. Sakamoto, T. Sengoku and H. Yoda, Controllable monobromination of perylene ring system: synthesis of bay-functionalized perylene dyes, *J. Org. Chem.*, 2018, **83**, 624–631.

21 M. Schulze, M. Philipp, W. Waigel, D. Schmidt and F. Würthner, Library of azabenz-annulated core-extended perylene derivatives with diverse substitution patterns and tunable electronic and optical properties, *J. Org. Chem.*, 2016, **81**, 8394–8405.

22 R. Gupta and A. Achalkumar, Microwave-assisted method for the synthesis of perylene ester imides as a gateway toward unsymmetrical perylene bisimides, *J. Org. Chem.*, 2018, **83**, 6290–6300.

23 R. Gupta, A. Dey, A. Singh, P. Iyer and A. Sudhakar, Heteroatom bay-annulated perylene bisimides: new materials for organic field effect transistors, *ACS Appl. Electron. Mater.*, 2019, **1**, 1378–1386.

24 F. Zhang, W. Dong, Y. Ma, T. Jiang, B. Liu, X. Li, Y. Shao and J. Wu, Fluorescent pH probes for alkaline pH range based on perylene tetra-(alkoxycarbonyl) derivatives, *Arabian J. Chem.*, 2020, **13**, 5900–5910.

25 C. Zhan, Y. Y. Jiang, M. Y. Yang, L. H. Lu and S. Q. Xiao, Synthesis and optoelectronic properties of a novel molecular semiconductor of dithieno [5,6-b:11,12-b0] coronene-2,3,8,9-tetracarboxylic tetraester, *Chin. Chem. Lett.*, 2014, **25**, 65–68.

26 A. Sedgwick, L. Wu, H. Han, S. Bull, X. He, T. James, J. Sessler, B. Tang, H. Tian and J. Yoon, Excited-state intramolecular proton-transfer (ESIPT) based fluorescence sensors and imaging agents, *Chem. Soc. Rev.*, 2018, **47**, 8842–8880.

27 F. Zhang, Y. Zhao, Y. Chi, Y. Ma, T. Jiang, X. Wei, Q. Zhao, Z. Shi and J. Shi, Novel fluorescent probes for the fluoride anion based on hydroxy-substituted perylene tetra-(alkoxycarbonyl) derivatives, *RSC Adv.*, 2018, **8**, 14084–14091.

28 G. Li, Y. Zhao, J. Li, J. Cao, J. Zhu, X. Sun and Q. Zhang, Synthesis, characterization, physical properties, and OLED application of single BN-fused perylene diimide, *J. Org. Chem.*, 2015, **80**, 196–203.

29 Y. Ma, Y. Zhao, F. Zhang, T. Jiang, X. Wei, H. Shen, R. Wang and Z. Shi, Two new chemosensors for fluoride ion based on perylene tetra-(alkoxycarbonyl) derivatives, *Sens. Actuators, B*, 2017, **241**, 735–743.

30 K. K. Ong, J. O. Jensen and H. F. Hameka, Theoretical studies of the infrared and Raman spectra of perylene, *J Mol Struct Theochem*, 1999, **459**, 131–144.

31 A. D. Becke, Density-functional exchange-energy approximation with correct asymptotic behavior, *Phys. Rev. B*, 1998, **38**, 3098–3100.

32 A. D. Becke, Density-functional thermochemistry. III. The role of exact exchange, *J. Phys. Chem.*, 1993, **98**, 5648–5652.

33 R. Wang, J. Li, G. Li, C. Hao, Y. Zhang, S. Wang, J. Zhao, Q. Liu and Z. Shi, Synthesis of 1-amino-12-hydroxyl-perylene tetra-(alkoxycarbonyl) for selective sensing of fluoride, *Dyes Pigm.*, 2018, **156**, 225–232.

34 J. Vollbrecht, C. Wiebeler, A. Neuba, H. Bock, S. Schumacher and H. Kitzerow, Bay-extended, distorted perylene esters showing visible luminescence after ultraviolet excitation: photophysical and electrochemical analysis, *J. Phys. Chem. C*, 2016, **120**, 7839–7848.

35 A. Amalraj and A. Pius, Chemosensor for fluoride ion based on chromone, *J. Fluorine Chem.*, 2015, **178**, 73–78.

36 V. K. Gupta, N. Mergu, L. K. Kumawat and A. K. Singh, A reversible fluorescence off–on–off sensor for sequential detection of aluminum and acetate/fluoride ions, *Talanta*, 2015, **144**, 80–89.

37 G. Boobalan, P. M. Imran, S. G. Ramkumar and S. Nagarajan, Fabrication of luminescent perylene bisimide nanorods, *J. Lumin.*, 2014, **146**, 387–393.

38 C. Parthiban and K. Elango, Amino-naphthoquinone and its metal chelates for selective sensing of fluoride ions, *Sens. Actuators, B*, 2015, **215**, 544–552.

39 R. Ali, S. Razi, R. Gupta, S. Dwivedi and A. Misra, An efficient ICT based fluorescent turn-on dyad for selective detection of fluoride and carbon dioxide, *New J. Chem.*, 2016, **40**, 162–170.

40 A. Satheshkumar and K. P. Elango, Spectral and DFT studies on simple and selective colorimetric sensing of fluoride ions via enhanced charge transfer using a novel signaling unit, *Dyes Pigm.*, 2013, **96**, 364–371.

41 P. Anzenbacher, M. A. Palacios, K. Jursikova and M. Marquez, Simple electrooptical sensors for inorganic anions, *Org. Lett.*, 2005, **7**, 5027–5030.